Protein–Protein Interactions Hot Paper

International Edition: DOI: 10.1002/anie.201507976
German Edition: DOI: 10.1002/ange.201507976

Stabilizer-Guided Inhibition of Protein–Protein Interactions

Lech-Gustav Milroy, Maria Bartel, Morkos A. Henen, Seppe Leysen, Joris M. C. Adriaans, Luc Brunsveld, Isabelle Landrieu,* and Christian Ottmann**

Abstract: *The discovery of novel protein–protein interaction (PPI) modulators represents one of the great molecular challenges of the modern era. PPIs can be modulated by either inhibitor or stabilizer compounds, which target different though proximal regions of the protein interface. In principle, protein–stabilizer complexes can guide the design of PPI inhibitors (and vice versa). In the present work, we combine X-ray crystallographic data from both stabilizer and inhibitor co-crystal complexes of the adapter protein 14-3-3 to characterize, down to the atomic scale, inhibitors of the 14-3-3/Tau PPI, a potential drug target to treat Alzheimer's disease. The most potent compound notably inhibited the binding of phosphorylated full-length Tau to 14-3-3 according to NMR spectroscopy studies. Our work sets a precedent for the rational design of PPI inhibitors guided by PPI stabilizer–protein complexes while potentially enabling access to new synthetically tractable stabilizers of 14-3-3 and other PPIs.*

Protein–protein interaction (PPI) modulators hold great promise for 21st century drug discovery.[1] Extensive efforts over the last quarter century have transformed PPI inhibition into a viable therapeutic strategy,[1a,c] but left PPI stabilization underexploited until recently.[1d,2] Studies on the adaptor protein 14-3-3 have shown that whereas PPI inhibitors compete with client proteins, PPI stabilizers target proximal regions of the protein–protein interface (e.g., Figure 1 a).[3,4] Therefore, both forms of modulation provide complementary structural information on the potential druggability of a target PPI, which may prove to be useful for the rational optimization of inhibitors and potentially even the design of stabilizer compounds.

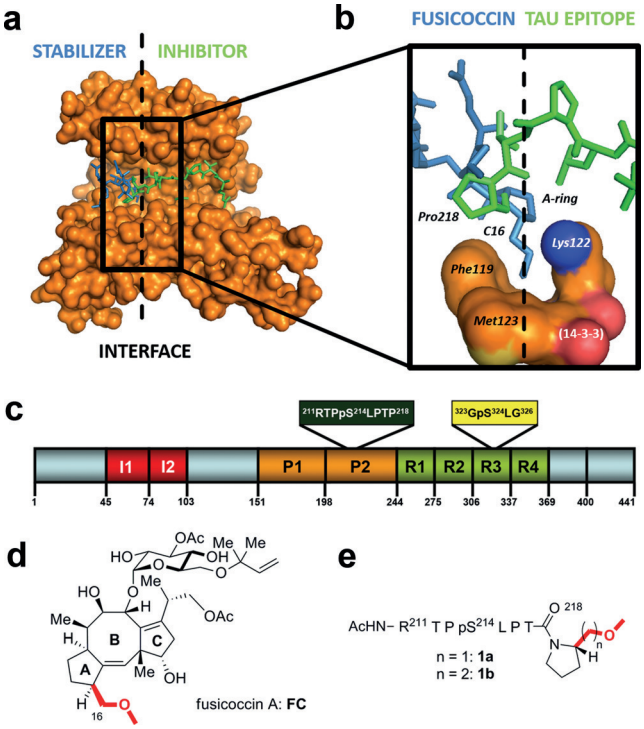

Figure 1. a) PPI stabilizer (blue) and inhibitor (green) space of 14-3-3 (orange). b) Enlarged image of the stabilizer/inhibitor interface of 14-3-3σ/Tau (PDB No. 4FL5) and 14-3-3σ/FC (PDB No. 3P1Q). c) Tau domain structure and its two 14-3-3 binding epitopes[7] in P2 and R3. d) Structure of stabilizer FC. e) The 14-3-3/Tau inhibitors **1a** and **1b** (Scheme 1) with the grafted FC moiety highlighted in red.

[*] Dr. L.-G. Milroy, Dr. M. Bartel, Dr. S. Leysen, J. M. C. Adriaans, Prof. Dr. L. Brunsveld, Dr. C. Ottmann
Laboratory of Chemical Biology and Institute of Complex Molecular Systems (ICMS), Department of Biomedical Engineering
Technische Universiteit Eindhoven
Den Dolech 2, 5612 AZ Eindhoven (The Netherlands)
E-mail: l.milroy@tue.nl
c.ottmann@tue.nl

Dr. M. A. Henen, Dr. I. Landrieu
UMR 8576 CNRS-Lille University
59000 Villeneuve O'Ascq (France)
E-mail: isabelle.landrieu@univ-lille1.fr

Dr. C. Ottmann
Department of Chemistry, University of Duisburg-Essen
Universitätsstrasse 7, 45117 Essen (Germany)

Supporting information (peptide synthesis, fluorescence anisotropy, surface plasmon resonance, isothermal calorimetry, X-ray crystallography, LC-ESI-MS and ESI-QTOF-MS analyses, ^{1}H and ^{1}H–^{15}N HSQC NMR spectroscopy) for this article is available on the WWW under http://dx.doi.org/10.1002/anie.201507976.

Our interest in this work originates from ongoing efforts to establish 14-3-3/Tau[5,6] as a drug target to treat Alzheimer's disease (AD).[7] According to the WHO, 36 million people were suffering from dementia worldwide in 2010[8,9]—a figure set to triple by 2050—with a striking 80% of the US $604 billion treatment costs in 2010 assigned to social care. New therapeutic approaches are therefore needed to treat dementia. The microtubule-binding protein, Tau, has been implicated in the development of AD,[10] and Tau hyperphosphorylation (pTau) has been shown to enhance the formation of neurofibrillary tangles (NFTs) by disrupting Tau binding to microtubules.[11] The adaptor protein 14-3-3[12,13] regulates Tau phosphorylation[14] through binding to pTau at two epitope sites, pS214 and pS324 (Figure 1 c).[7] We previously showed that 14-3-3 binding to Tau destabilizes tubulin and blocks axon development through inhibition of pTau binding to microtubules,[7] and that pharmacological intervention of 14-3-3/Tau may be a beneficial strategy to treat AD.

Herein, we report the first rational design of a PPI inhibitor that was guided by the X-ray co-crystal structure of a protein–stabilizer complex. We synthesized chimeric inhibitors of 14-3-3/Tau based on the Tau pS214 epitope (hereafter "Tau epitope") that specifically target modifications at the stabilizer/inhibitor interface of the PPI (Figure 1a,b). We initially screened the activity of our compounds in a fluorescence anisotropy assay and then through extensive biophysical studies, including X-ray co-crystallography and NMR spectroscopy, and characterized a potent 14-3-3/Tau inhibitor that exhibited notable activity against full-length Tau.

During a preliminary evaluation of different 14-3-3 co-crystal complexes, we identified significant overlap between the C-terminal Pro218 residue of the Tau epitope and the A-ring of fusicoccin A (FC; Figure 1b) on superposition of the co-crystal structures of 14-3-3/Tau (PDB No. 4FL5) and 14-3-3/FC (PDB No. 3P1Q). FC stabilizes 14-3-3 binding to the plant plasma membrane H^+-ATPase through simultaneous contacts with both protein partners.[15] Important for FC binding is the C16 *O*-methoxy substituent (OMe) group (Figure 1d), which targets the highly conserved hydrophobic (FC) pocket, formed by residues Phe, Met, and Lys, within the amphiphilic groove of the protein (Figure 1b). We hypothesized that grafting the OMe group to the Tau epitope (e.g., **1a** and **1b**; Figure 1e) would increase ligand affinity by addressing the FC pocket.

We synthesized homologues **1a** and **1b** using the solid-phase approach delineated in Scheme 1. For the amide coupling step (Scheme 1, step a), initial attempts using (benzotriazol-1-yloxy)tripyrrolidinophosphonium hexafluorophosphate (PyBOP) as the coupling reagent and DIPEA in general resulted in only low conversion into the desired product. A switch to PyClock (see the Supporting Information) led to higher product formation and cleaner crude material (LC-MS) after global deprotection using TFA.[16] In subsequent fluorescence anisotropy studies, the Tau epitope exhibited only weak activity (Table 1 and Figure 2a) whereas compounds **1a** and **1b** were stronger inhibitors with IC_{50} values of 83 and 90 μM, respectively. We solved the co-crystal structure of analogue **1b** bound to 14-3-3σ at 1.7 Å resolution (Figure 3a, PDB No. 4Y32) and observed that as with the unmodified Tau epitope (PDB No. 4FL5), the peptidic region of **1b** binds to the amphiphilic groove of 14-3-3 in a canonical extended manner. Significantly, the FC-derived OMe group of **1b** is bound to the FC pocket, which provides a clear molecular explanation for the enhanced activity of **1a** and **1b** compared to the unmodified Tau epitope.

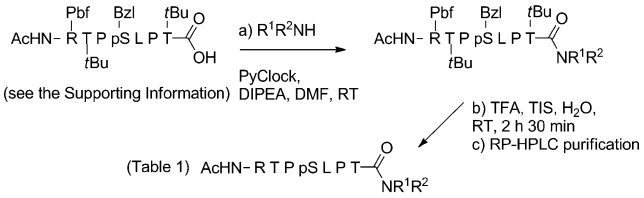

Scheme 1. Synthesis of chimeric inhibitors (see also Table 1 and the Supporting Information). Bzl = benzyl, DIPEA = *N*,*N*-diisopropylethylamine, Pbf = 2,2,4,6,7-pentamethyldihydrobenzofuran-5-sulfonyl, TFA = trifluoroacetic acid, TIS = triisopropylsilane.

Table 1: Structure and activity of chimeric inhibitors (see Scheme 1).

R^1R^2NH	Analogue	IC_{50} [μM] (±)[b]
–[a]	Tau epitope	ca. 1330.0
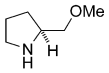	**1a**	83.1 (1.0)
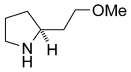	**1b**	90.1 (1.0)
	**2a**	301.3 (1.0)
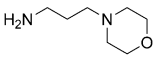	**2b**	178.5 (1.1)
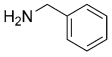	**2c**	55.4 (1.1)
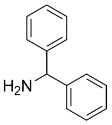	**3a**[c]	60.1 (1.5)
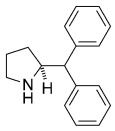	**3b**	5.9 (1.0)

[a] Structure of the Tau epitope: AcNH-RTPpSLPTP-OH.[7] [b] See Figure 2a; determined by fluorescence depolarization using a fluorescein (FAM) labeled diphosphorylated peptide derived from the two predominant 14-3-3 binding epitopes of Tau (Figure 1c). [c] Result for a sample enriched with the major diastereomer of **3a** (Figure S4).[16]

We next employed the phosphorylated Tau epitope as a non-covalent tether to probe the FC pocket (Table 1, analogues **2a**–**2c** and **3a**, **3b**). Analogue **2a**, which lacks the OMe group, was more than threefold less active than **1a** and **1b**. The co-crystal structure of **2a** in complex with 14-3-3σ (solved at 1.4 Å resolution) can be used to explain this activity drop in terms of the absence of a stabilizing hydrophobic interaction between peptide and protein, specifically at the FC pocket (Figure 3b, PDB No. 4Y5I). This structure–activity relationship fits coherently with the data for analogues **1a** and **1b** and the unmodified Tau epitope, and provides further evidence for the stabilizing effect of the FC-derived OMe group on the Tau epitope. Replacing the *N*′,*N*′-disubstituted secondary amide with a primary amide, as in **2b** (Table 1), led to a nearly twofold increase in inhibitory activity compared to **2a**. In this case, the flexible hydrophobic linker and the bulky six-membered ring may occupy more of the amphipathic groove, but not specifically address the FC pocket. Finally, *N*-benzyl amide **2c** (Table 1) was more active than **2a** by a modest, though significant factor of 5.5 (IC_{50} = 55 μM).

The result for **2c** suggests that introducing bulky aromatic groups to the Tau epitope would enhance the binding affinity by addressing more of the FC pocket. We therefore synthesized the benzhydryl derivatives **3a** and **3b** (Table 1). Initially,

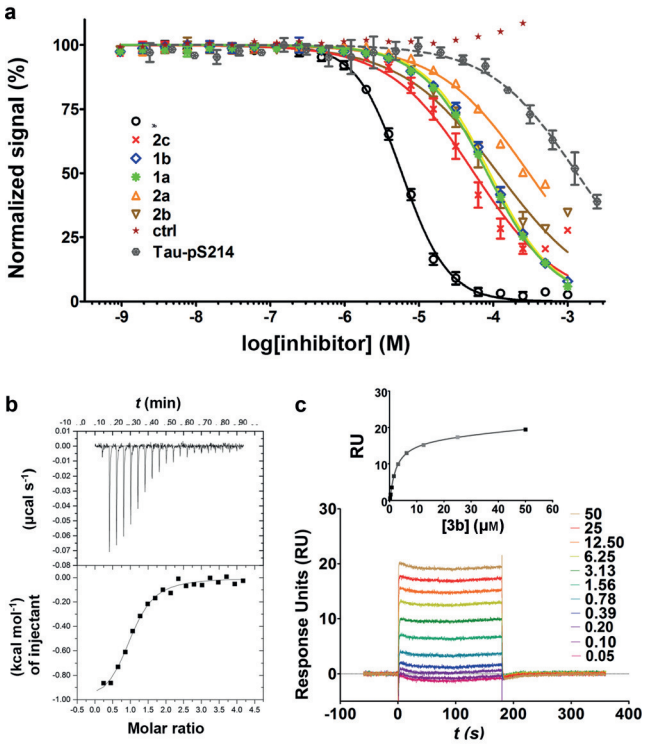

Figure 2. Biophysical activities of chimeric 14-3-3/Tau inhibitors. a) Titration of compounds on FAM-labeled diphosphorylated competitor peptide in the presence of 10 μM of the 14-3-3 protein and subsequent anisotropy measurements; see Figure S4 for F data on **3a**. b) Isothermal titration calorimetry (ITC) of the direct binding of **3b** to 14-3-3 ($K_d = 13.4 \pm 5.02$ μM). c) Surface plasmon resonace (SPR) analysis: The biotinylated 14-3-3 protein was immobilized on a streptavidin-coated gold surface and titrated with **3b** ($K_d = 2.2 \pm 0.09$ μM).

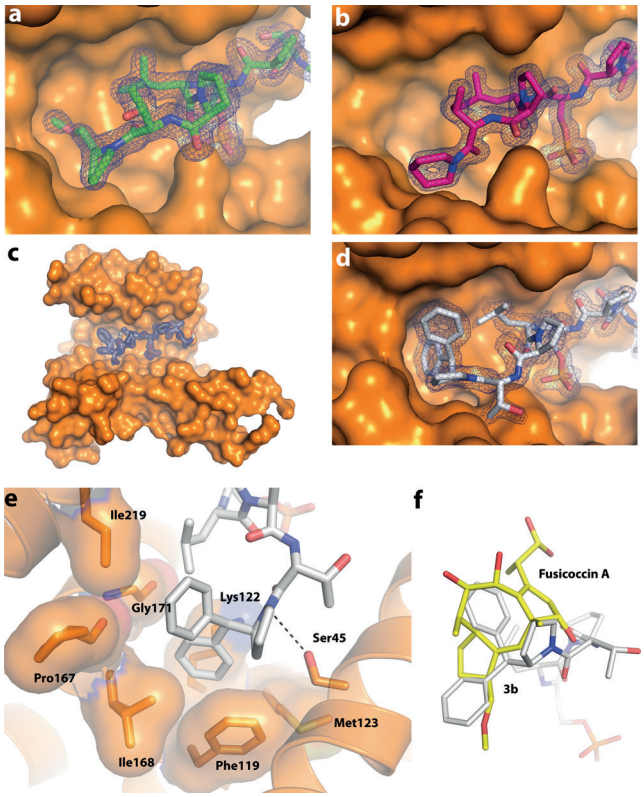

Figure 3. Binding of the chimeric inhibitors to 14-3-3σ. Electron densities ($2F_o - F_c$, contoured at 1σ) of **1b** (a; green, blue, and red sticks, PDB No. 4Y32) and **2a** (b; mauve and blue, PDB ID No. 4Y5I) bound to 14-3-3σ (orange solid surface. c) Electron density ($2F_o - F_c$, contoured at 1σ) of **3b** (white, blue, and red sticks, PDB No. 4Y3B) bound to 14-3-3σ (orange solid surface). d) Enlarged view of (c). e) Residues of 14-3-3σ directly accommodating modification of the Tau–pS214 recognition motif in **3b**. Residues that contribute to the hydrophobic contact surface are shown as orange sticks with a semi-transparent surface and polar contacts as black dotted lines. f) Structural superposition of **3b** (white sticks) and FC (yellow and red sticks) bound to 14-3-3σ using PDB No. 3IQV as the template.

we found the benzhydryl amide analogue **3a** to be equipotent to **2c** (Table 1 and Figure S4), suggesting that a second phenyl ring would be accommodated at the inhibitor–stabilizer interface of 14-3-3. Subsequently, appending the peptide C-terminus with the sterically bulky and conformationally rigid benzhydryl pyrrolidine moiety **3b** (Table 1) led to a further tenfold increase in activity relative to **2c** (Figure 2a). Subsequent ITC and SPR studies on **3b** concluded with measured K_d values of 13.4(±5.02) and 2.2(±0.09) μM, respectively (Figure 2b,c), which are in good agreement with the fluorescence anisotropy data for this analogue. To gain insight into the molecular details of the interaction, we solved the crystal structure of **3b** bound to 14-3-3σ at 1.8 Å resolution (Figure 3c,d, PDB No. 4Y32). Intriguingly, and contrary to our expectations, the electron density at the C-terminus was highly characteristic of the binding of a diastereomer of **3b**, namely an epimer that is *R*-configured at the α-stereocenter of the C-terminal threonine residue instead of the expected *S*-configured epimer (Figure 3c,d and Figure S18). In this case, the natural *S* epimer of **3b** is most likely the major product and the *R* epimer a minor impurity that is formed during the synthesis of **3b**, specifically through epimerization during the solution-phase amide coupling step (see the Supporting Information for a more detailed discussion).[16]

Nevertheless, the binding preference of the *R* epimer may serve as a potentially useful indicator for future ligand design. Furthermore, the data for **3b** made us aware of the specific contribution of the benzhydryl pyrrolidine moiety towards a near 1000-fold increase in binding affinity through a specific interaction at the FC pocket. While the first phenyl ring of **3b** is more exposed to bulk solvent, the second phenyl ring is excluded from bulk solvent and occupies the FC pocket more fully than the OMe group of **1b** (Figure 3e), thus providing a clear molecular explanation for the increased activity of **3b** that was observed during the fluorescence anisotropy studies. Crucially, the binding of the benzhydryl pyrrolidine moiety is FC-like (Figure 3f and Figure S19).

To assess the potential of 14-3-3/pTau (PKA-phosphorylated Tau) inhibition under more physiologically relevant conditions, we performed NMR spectroscopic studies on 14-3-3ζ and full-length Tau in the presence and absence of **3b** (Figure 4). Here, the intensity I of correlation signals of ^{15}N pTau were monitored in a pair of spectra (I and I0), where binding of 14-3-3ζ led to peak broadening and loss of

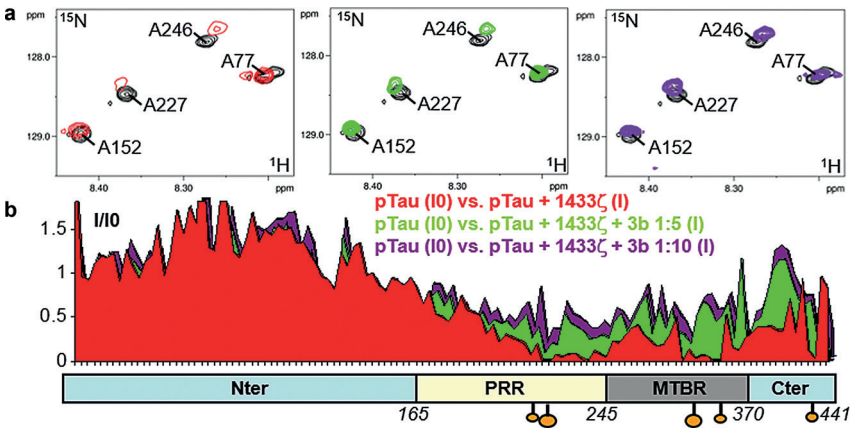

Figure 4. Characterization of 14-3-3ζ binding to full-length PKA-phosphorylated Tau (pTau) at different pTau/14-3-3/**3b** ratios by NMR spectroscopy. a) Selected enlarged regions of overlaid 2D spectra; ^{15}N resonances on the *y* axis, ^{1}H resonances on the *x* axis. The resonances of free pTau are shown in black. b) Plot of the intensity ratios (I/I0) of the ^{1}H–^{15}N correlation signals (*y* axis) versus the amino acid sequence (*x* axis) for full-length pTau in the absence (I0) or presence (I) of 14-3-3ζ or for different ratios of 14-3-3ζ/**3b** (a total of 120 correlation peak intensities are shown). The *x* axis is not proportional. The domains of Tau were delineated and correspond, aside from the N- and C-terminal regions, to the proline-rich region (PRR) and the microtubule binding region (MTBR). Phosphorylation sites are indicated along the scheme by orange dots; larger orange dots indicate stronger phospho-epitope sites, pS214 and pS324, while smaller dots indicate weaker phospho-epitope sites; pTau (60 μM), 14-3-3ζ (120 μM), DMSO (5%), 298 K, pH 6.7.

intensity, and thus a decrease in the calculated I/I0 ratio.[16] For pTau, the intensity ratios reported along the sequence were highest in non-epitope regions (Figure 4, N-terminal region of Tau) and in general lowest at and in the locality of the two main phospho epitope sites pS214 and pS324 (Figures 1c and 4),[7] thereby indicating attachment of 14-3-3ζ at these two sites. The addition of **3b** to the pTau/14-3-3ζ complex resulted in a dose-dependent increase in I/I0 corresponding to residues located in the interaction domain in and about the stronger epitope sites pS214 and pS324 (Figure 4). An additional bimodal effect was detected upon addition of **3b** (Figure 4) as the intensity recovery was proportionally more important in the C-terminal region, probably owing to the efficient disruption of the interaction of 14-3-3ζ with the weaker phospho epitopes (pS356 and pS416, Figure S20) by **3b**. The addition of **3b** had little effect on 14-3-3ζ binding to non-phosphorylated Tau (Figure S21). Based on these data, we conclude that **3b** inhibits the binding of 14-3-3ζ to phosphorylated full-length Tau. The interaction region of Tau with the microtubules that was previously defined by NMR spectroscopy is similar to the region here defined to be immobilized by 14-3-3 binding.[17,18] It can be expected that if detachment of Tau from 14-3-3, stimulated by a **3b**-derived compound, were ever to occur in a cellular environment, for example, then this region would be freed for microtubule binding, which may restore neurite growth further downstream.[7] Probing the entire 14-3-3 interactome for specificity, by proteomics methods, for example, is clearly an important next step towards realizing true therapeutic options based on the 14-3-3/Tau interaction. By acting on the full-length phosphorylated Tau protein, our most potent inhibitor, **3b**, has realized a first step towards addressing 14-3-3/Tau specificity.

In conclusion, we have disclosed the first rational design of a PPI inhibitor that was guided by the co-crystal structure of a protein–stabilizer complex, culminating in the biochemical and structural characterization of a potent inhibitor of 14-3-3/Tau that is capable of inhibiting phosphorylated full-length Tau. The close interplay between chemical synthesis and X-ray crystallography is key to the efficient optimization of compound activity. Studies are ongoing to improve the metabolic stability and cell permeability of our probe compound to facilitate studies on 14-3-3/Tau inhibition in cells. We argue that the crystal structure of a protein–stabilizer complex has never before been used to rationally optimize the binding properties of a PPI inhibitor (or vice versa), owing to the lack of high-resolution structural information on PPI stabilizers. Furthermore, the non-covalent tethering approach used here has helped to characterize a new molecular structure targeting the stabilizer/inhibitor interface of 14-3-3. The benzhydryl pyrrolidine moiety present in **3b**, aside from contributing to a near 1000-fold increase in 14-3-3 binding affinity compared to the unmodified Tau epitope, also represents a new molecular scaffold that may enable access to novel synthetically tractable non-phosphorylated inhibitors and stabilizers of 14-3-3.

Acknowledgements

We thank Lotte van Beek, Job Roodhuizen, Gerwin Salentijn, and Gael Vos for help with compound synthesis and biochemical characterization, François-Xavier Cantrelle for NMR data acquisition, and Joost van Dongen and Dr. Xianwen Lou for help with ESI-QTOF-MS measurements. All X-ray crystal structure images were prepared using PyMOL (The PyMOL Molecular Graphics System, Version 1.7.4 Schrödinger, LLC). Funding was granted by the Netherlands Organization for Scientific Research (Gravity program 024.001.035), Marie Curie Action (PIAPP-GA-2011-286418 14-3-3Stabs to M.A.H. and S.L.), and the LabEx (Laboratory of Excellence) DISTALZ program (ANR, ANR-11-LABX-009). The NMR facilities were financially supported by the North of France Region, CNRS, the Pasteur Institute of Lille, the European Community through FEDER, the French Research Ministry, and Lille University. We acknowledge support from TGE RMN THC (FR-3050, France). A part of this work has been reported in the PhD thesis of Dr. Maria Bartel (ISBN: 978-90-386-3858-4).

Keywords: drug discovery · peptide inhibitors · protein–protein interactions · structure-guided design

How to cite: *Angew. Chem. Int. Ed.* **2015**, *54*, 15720–15724
Angew. Chem. **2015**, *127*, 15946–15950

[1] a) M. R. Arkin, J. A. Wells, *Nat. Rev. Drug Discovery* **2004**, *3*, 301–317; b) J. A. Wells, C. L. McClendon, *Nature* **2007**, *450*, 1001–1009; c) M. R. Arkin, Y. Tang, J. A. Wells, *Chem. Biol.* **2014**, *21*, 1102–1114; d) L. G. Milroy, T. N. Grossmann, S. Hennig, L. Brunsveld, C. Ottmann, *Chem. Rev.* **2014**, *114*, 4695–4748.
[2] a) M. Bartel, A. Schäfer, L. M. Stevers, C. Ottmann, *Future Med. Chem.* **2014**, *6*, 903–921; b) P. Thiel, M. Kaiser, C. Ottmann, *Angew. Chem. Int. Ed.* **2012**, *51*, 2012–2018; *Angew. Chem.* **2012**, *124*, 2052–2059.
[3] a) C. Anders et al., *Chem. Biol.* **2013**, *20*, 583–593; b) I. J. de Vries-van Leeuwen et al., *Proc. Natl. Acad. Sci. USA* **2013**, *110*, 8894–8899; c) M. Molzan et al., *ACS Chem. Biol.* **2013**, *8*, 1869–1875.
[4] P. Block, N. Weskamp, A. Wolf, G. Klebe, *Proteins Struct. Funct. Bioinf.* **2007**, *68*, 170–186.
[5] J. Chun et al., *Mol. Cells* **2004**, *18*, 360–368.
[6] C. Johnson, S. Crowther, M. J. Stafford, D. G. Campbell, R. Toth, C. MacKintosh, *Biochem. J.* **2010**, *427*, 69–78.
[7] Y. Joo et al., *FASEB J.* **2015**, *29*, 4133–4144.
[8] Dementia: a public health priority, World Health Organization, 2012, ISBN: 978 92 4 156445 8.
[9] M. Wortmann, *Alzheimers Res. Ther.* **2012**, *4*, 40.
[10] E. Giacobini, G. Gold, *Nat. Rev. Neurol.* **2013**, *9*, 677–686.
[11] K. Iqbal, F. Liu, C.-X. Gong, A. D. C. Alonso, I. Grundke-Iqbal, *Acta Neuropathol.* **2009**, *118*, 53–69.
[12] A. Aitken, *Semin. Cancer Biol.* **2006**, *16*, 162–172.
[13] M. B. Yaffe et al., *Cell* **1997**, *91*, 961–971.
[14] M. Hashiguchi, K. Sobue, H. K. Paudel, *J. Biol. Chem.* **2000**, *275*, 25247–25254.
[15] M. Würtele, C. Jelich-Ottmann, A. Wittinghofer, C. Oecking, *EMBO J.* **2003**, *22*, 987–994.
[16] See the Supporting Information for an extended discussion.
[17] A. Sillen et al., *Biochemistry* **2007**, 46, 3055–3064.
[18] H. Kadavath et al., *Proc. Natl. Acad. Sci. USA* **2015**, *112*, 7501–7506.

Received: August 25, 2015
Revised: September 23, 2015
Published online: November 5, 2015

